Applied Catalysis B: Environmental 239 (2018) 475–484

Contents lists available at ScienceDirect

Applied Catalysis B: Environmental

journal homepage: www.elsevier.com/locate/apcatb

Highly selective photocatalytic production of H_2O_2 on sulfur and nitrogen co-doped graphene quantum dots tuned TiO_2

Longhui Zheng[a], Hanrui Su[a], Jingzhen Zhang[a], Laxman S. Walekar[a], Hamed Vafaei Molamahmood[a], Baoxue Zhou[a], Mingce Long[a,b,*], Yun Hang Hu[a]

[a] School of Environmental Science and Engineering, Shanghai Jiao Tong University, 800 Dongchuan Road, Shanghai 200240, China
[b] Key Laboratory of Thin Film and Microfabrication Technology (Ministry of Education), Shanghai Jiao Tong University, 800 Dongchuan Road, Shanghai 200240, China

ARTICLE INFO

Keywords:
Photocatalysis
H_2O_2
Graphene quantum dots
Two-electron pathway
Oxygen reduction reaction

ABSTRACT

Photocatalytic production of hydrogen peroxide (H_2O_2) using water and molecular oxygen as the sole material source is a promising and sustainable solar fuel approach. Herein, we developed an efficient photocatalyst (SN-GQD/TiO_2) for H_2O_2 syntheses by tuning TiO_2 with sulfur and nitrogen co-doped graphene quantum dots (SN-GQDs). The high luminescent SN-GQDs homogeneously dispersed on TiO_2 surface, which induces the extended visible light absorption and enhanced electron migration. The SN-GQD/TiO_2 exhibited 3.2 times H_2O_2 yield (451 μmol L^{-1}) as that of bare TiO_2 under simulated sunlight irradiation, which was also significantly higher than that over GQD/TiO_2 and N-GQD/TiO_2. Kinetic evaluations suggested that the formation of H_2O_2 on SN-GQD/TiO_2 was dramatically accelerated by 2.4 times compared with that on TiO_2, while the decomposition of H_2O_2 was moderately suppressed (only 25% reduction). The increased H_2O_2 formation on SN-GQD/TiO_2 was attributed to the boosted two-electron reduction of oxygen, which was confirmed by the electron transfer numbers (n = 2.2) obtained from Koutecky-Levuch plots, the less sensitivity of H_2O_2 production to pH, and the insignificant signals for DMPO–$O_2\cdot^-$ in ESR measurements. According to theoretical calculations and free energy diagrams of the ORR pathway, a mechanism of proton-coupled electron transfer (PCET) to produce H_2O_2 was proposed to understand the highly selective two-electron H_2O_2 production on SN-GQD/TiO_2. This study brings an insight to modulate highly selective two-electron photocatalytic reduction of oxygen by introduction of dual doped GQDs that can provide active sites for *OOH formation and proton relays.

1. Introduction

Hydrogen peroxide (H_2O_2) has been widely used as a multi-purpose environmental friendly oxidant in biological process, water purification and chemical industry since it only emits water as a final byproduct [1–4]. There are two main technologies for industrial production of H_2O_2: anthraquinone oxidation [1] and direct synthesis from H_2 and O_2 [5,6]. The former process is limited by high energy input and tedious steps for multiple hydrogenation and oxidation reactions [1]. Furthermore, the mixture of H_2 and O_2 in the direct catalytic production of H_2O_2 in the latter approach raises the risk of explosion [7]. Therefore, it is still challengeable but highly demanding to produce H_2O_2 in a facile, clean, and safe way.

Recently, a great interest has been devoted to production of H_2O_2 by photocatalytic methods due to their well-known advantages, such as utilizing water and oxygen as the main material sources and sunlight as input energy [8–17]. It is generally recognized that excitation of photocatalysts produces electron (e^-) and hole (h^+) pairs, in which holes oxidize hydrogen donor (such as alcohols) causing the generation of oxidation products and protons (Eq. (1)); furthermore, electrons promote one-electron reduction of O_2 and produce H_2O_2 in sequential reactions (Eqs. (2) and (3)) [18]. Various photocatalysts with novel compositions and structures have been extensively explored for H_2O_2 production, such as graphitic C_3N_4 [19–22], $BiVO_4$ [23–25], $Cd_3(C_3N_3S_3)_2$ coordination polymer [26,27], CdS/graphene [28], up-conversion photocatalytic hybrids [29], and polymer-supported CQDs [30]. However, titanium dioxide (TiO_2) is still one of the most frequently investigated and promising photocatalysts due to its low cost and high stability [31]. Nevertheless, the efficiency of H_2O_2 production on TiO_2 is far from satisfactory levels. During photocatalytic production of H_2O_2 in TiO_2 suspensions, the adsorbed hydrogen peroxide in the form of $\equiv Ti-OOH$ complexes can be oxidized into oxygen either directly by photogenerated holes under UV irradiation or indirectly by injecting electrons to the conduction band (CB) of TiO_2 under visible

* Corresponding author at: School of Environmental Science and Engineering, Shanghai Jiao Tong University, 800 Dong Chuan Road, Shanghai 200240, China.
E-mail address: long_mc@sjtu.edu.cn (M. Long).

https://doi.org/10.1016/j.apcatb.2018.08.031
Received 4 June 2018; Received in revised form 4 August 2018; Accepted 13 August 2018
Available online 16 August 2018
0926-3373/

light irradiation (Eqs. (4) and (5)) [18,32]. Simultaneously, the predominant one-electron reduction of O_2 on TiO_2 surface results in the inherent low efficiency of oxygen reduction reaction (ORR) and H_2O_2 production, which was always regarded as the rate-determine step in TiO_2 photocatalysis [18,33]. Therefore, efficient photocatalytic H_2O_2 production requires selective promotion of two-electron reduction of O_2 and suppression of subsequent photodecomposition of the formed H_2O_2.

$$R - CH_2OH + 2h^+ \rightarrow R - CHO + 2H^+ \quad (1)$$

$$O_2 + e^- \rightarrow O_2^{\bullet -} \xrightarrow{H^+} HO_2^{\bullet} \quad (2)$$

$$HO_2^{\bullet} + H^+ + e^- \rightarrow H_2O_2 \quad (3)$$

$$\equiv Ti - OOH + hv \rightarrow \equiv Ti - \bullet OOH \rightarrow \equiv Ti - OH + 1/2\,O_2\ (Visible\ light) \quad (4)$$

$$\equiv Ti - OOH + 2h^+ + H_2O \rightarrow \equiv Ti - OH + O_2 + 2H^+\ (UV\ light) \quad (5)$$

Several strategies of surface modification have been developed to increase the photocatalytic production of H_2O_2 on TiO_2. Surface complexation with zinc(II) [12], copper (II) cations [10], or surface fluorination by forming Ti≡F groups [11], can block surface −OH sites and inhibit the formation of $\equiv Ti - OOH$ complexes, efficiently suppressing the decomposition and improving the production of H_2O_2. Surface loading noble metal nanoparticles, like Au-Ag bimetallic alloy, would not only promote the separation of photogenerated electron-hole pairs, but also suppress adsorption and decomposition of H_2O_2 [13]. Furthermore, H_2O_2 production without organic hole surface scavengers was facilitated by an in-situ formation of cobalt phosphate on reduced graphene oxide (rGO)/TiO_2 composite [14]. Although current surface modifications have achieved great success in suppression of H_2O_2 adsorption and decomposition, all of these systems exhibit insufficient selectivity for H_2O_2 production as a result of predominant one-electron ORR. To solve this issue, selective two-electron ORR in TiO_2 photocatalysis is necessary to be obtained.

Extensive studies have been conducted to develop low cost and high efficient ORR electrocatalysts in energy conversion and storage [34–36]. Among them, graphene based materials have become very popular candidates due to their large surface area, high conductivity and excellent mechanical properties [34,37,38]. Introduction of heteroatoms (like S and N) into the graphitic framework can generate non-neutral electronic distribution, favor adsorption of molecular oxygen, accelerate its subsequence reduction rate, and modulate electron transfer numbers in ORR [34]. Simultaneously, enormous efforts have been taken to explore graphene for fabricating high performance photocatalysts [39,40]. In addition to the common roles in the enhancement of photogenerated charge separation and the extension of light absorption range, graphene was recently found to boost a two-electron ORR pathway in the photocatalysis of WO_3 or TiO_2/WO_3 composites [41,42]. This indicates that graphene based materials are promising candidates to change ORR pathways for highly efficient H_2O_2 production.

Graphene quantum dots (GQDs) is an emerging member in the family of graphene based materials. It acquires unique properties derived from the atomically thin 2D structure of the graphene. Additionally, GQDs possess fluorescence properties that make them promising to extend the absorption band of wide band gap photocatalysts like TiO_2 [43–45]. Co-doping of heteroatoms with different electronegativity in GQDs has been frequently employed to change charge distribution, leading to surface passivation, and accordingly enhances the fluorescence performance and catalytic activity. Among them, N and/or S doped graphene and GQDs showed great enhanced catalytic ORR and luminescence performance [34,35,46–53]. However, to the best of our knowledge, doped GQDs has not been reported for photocatalytic production of H_2O_2. Herein, sulfur and nitrogen co-doped GQDs (SN-GQDs) was employed to tune TiO_2 as efficient catalyst (SN-GQD/TiO_2) for H_2O_2 production. Furthermore, the enhanced photocatalytic performance for production of H_2O_2 was observed, and the mechanism on the highly selective two-electron reduction of O_2 was discussed.

2. Experimental section

2.1. Materials

Sodium perchlorate ($NaClO_4$), phenol, 2-propanol, and *N,N*-diethyl-*p*- phenylenediamine (DPD, 97%) were purchased from Sigma Aldrich. 5,5-Dimethy-l-pyrroline *N*-oxide (DMPO) was obtained from Adamas Co., Ltd., China. Commercial Degussa P25 TiO_2 (a mixture of 71% anatase and 29% rutile) was employed throughout the experiments. Horseradish peroxidase (POD, RZ > 1.5) was obtained from the Sangon Biotech Co., Ltd., China. Besides, citric acid, thiourea, urea, KNO_3, HNO_3, NaOH and Al_2O_3 were provided by Sinopharm Group Co. Ltd.

2.2. Syntheses of photocatalysts

SN-GQDs solution was prepared by a hydrothermal method [52]. Briefly, 0.315 g (1.5 mmol) citric acid and 0.345 g (4.5 mmol) thiourea were dissolved into 7.5 mL water followed by stirring for 3 h to form a clear solution. Then, the solution was transferred into a 30 mL Teflon lined stainless autoclave and kept at 160 °C for 4 h. After centrifugation at 6000 rpm for 20 min, the supernatant was collected to obtain the final SN-GQDs solution. N-GQDs solution was prepared by the same procedure except using urea instead of thiourea as the nitrogen source, and GQDs solution was synthesized by only citric acid [49]. The final solutions of the three GQDs were diluted by 0.25 M NaOH, and their pHs were adjusted to 7.0 using 1 M $HClO_4$.

The composites were prepared with an impregnation method. In a typical procedure, SN-GQD/TiO_2 was prepared by mixing SN-GQDs and 1 g TiO_2 powder in a 10 mL solution at assigned volume and weight ratios of SN-GQDs and TiO_2. The final products were collected through filtration and dried at 60 °C for 24 h. A series of GQD/TiO_2 and N-GQD/TiO_2 composites with varied weight percentages of GQDs and N-GQDs were also prepared. The control sample, SN-GQD/Al_2O_3, was also synthesized using Al_2O_3 powder as the substrate, and the amount of SN-GQDs were 0.5 wt%.

2.3. Characterizations

High resolution-transmission electron microscopy (HR-TEM, Tecnai G^2 F20, FEI) was used to observe the morphologies of samples. X-ray photoelectron spectroscopy (XPS) spectra were collected on an Axis Ultra DLD spectrometer (Kratos Analytical-A Shimadzu, Japan) using a monochromatic Al K*α* source (1486.6 eV), and the overall instrument resolution was 0.48 eV. The weight percentages of doped or undoped GQDs in the final composites were obtained by determining the carbon content using an Elementar vario MACRO cube analyzer (Elementar Analysensysteme GmbH, Germany). UV–vis diffuse reflectance spectra (DRS) of catalysts were obtained on a Lambda 950 UV/vis spectrophotometer (PerkinElmer Instrument Co., Ltd., USA) and converted from reflection to absorption through the Kubelka–Munk method. Photoluminescence (PL) spectra of the composites was also measured on a fluorescence spectrometer (QM/TM/IM, PTI Co. Ltd., USA). The Raman spectra were measured on a Raman microscopy (DXR, Thermo Scientific, USA) at room temperature. The excitation wavelength was 633 nm. The samples were prepared by transferring drops of the SN-GQD/TiO_2 suspension with or without illumination on a microscope slide for analyses.

The electron spin resonance (ESR) signals for DMPO–$O_2^{\bullet -}$ adducts were recorded on an ESR spectrometer (MS 5000, Magent Tech, Germany) by using DMPO as the spin trap. The suspension of catalysts (0.5 g/L) in methanol was irradiated for 25 min under simulated

sunlight in the presence of DMPO (20 mM). A sample (about 0.5 mL) was extracted, filtered through a 0.22 μm PES filter, and immediately transferred to a flat quartz ESR cell for ESR measurements. The ESR settings were: center field, 3506 G; sweep width, 200 G; sampling time, 0.015 s; microwave frequency, 9.815 GHz; and microwave power, 15 mW.

The potential of quasi-Fermi levels (E_{FL}) of the photocatalysts were determined by a slurry method [54,55]. In a typical test, 20 mg catalysts and 10 mg methylviologen dichloride ($(MV)Cl_2$, > 98%, TCI) were added into a 40 mL 0.1 M KNO_3 aqueous solution, and then the suspension was flushed with N_2 during the test. The working and reference electrodes were a platinum plate and a saturated calomel electrode (SCE), respectively. The suspension was magnetically stirred and irradiated by a 500 W Xe lamp. The photovoltages were recorded at various pH values that were adjusted by HNO_3 or NaOH solutions.

2.4. Photocatalytic performance

Photocatalytic H_2O_2 production was performed in a mixture of water (47 ml) and 2-propanol (3 ml) containing 25 mg of catalyst in a quartz cuvette. The initial pH of the suspension was adjusted to 3.0 by 1 M $HClO_4$. The suspension was saturated by oxygen gas and irradiated by visible light (with a cutoff filter, $\lambda \geq 420$ nm) or simulated sunlight (with a cutoff filter, $\lambda \geq 300$ nm) using a 500 W Xenon lamp as a light source.

To investigate photocatalytic degradation of phenol or decomposition of H_2O_2, a 50 mL suspension of catalysts (0.5 g/L) was mixed in a quartz reaction vessel with phenol (10 mg/L) or H_2O_2 (0.7 mM). The initial pH values of the suspensions were adjusted to 3.0 with 1 M $HClO_4$. The suspension was kept in the dark for 30 min to achieve adsorption–desorption equilibrium; then, it was illuminated by visible light or simulated sunlight. The samples were withdrawn at predetermined times, filtered through a 0.22-μm nylon filter for further measurements. The concentration of H_2O_2 was determined using a modified DPD–POD method [41,56]. Phenol was analyzed by a high-performance liquid chromatography system (LC-2010AHT, Shimadzu) equipped with a C-18 column. Elution was carried out with a 70:30 (v/v) mixture of phosphoric acid solution (0.1 wt%) and methanol at a 0.9 mL/min flow rate, and the detection wavelength was 270 nm.

2.5. Electrochemical and ORR tests

Electrochemical measurements were conducted on an electrochemical workstation (CHI 760E Chenhua Instrument Company, Shanghai, China) in a conventional three-electrode configuration with a Pt wire and an Ag/AgCl electrode as counter and reference electrodes, respectively. The working electrode was prepared by coating a slurry of catalysts on a cleaned indium tin oxide glass substrate and then drying at 80 °C in air for 3 h. The slurry was prepared by dispersing the catalysts (0.2 g) in absolute ethanol (1 mL). In all tests, the available surface area of the working electrode for irradiation was 1 cm^2. The electrolyte was a 0.1 M $NaClO_4$ solution (pH = 3.5). It was purged with nitrogen for 20 min prior to each test and continuously purged during the measurements. Electrochemical impedance spectroscopy (EIS) was performed by applying an open circuit voltage bias (+0.2 V *vs* Ag/AgCl) and measured over the frequency range of 0.1–10^5 Hz at an AC amplitude of 5 mV. Photocurrent measurements were conducted using the same three-electrode configuration by using the 500 W Xe lamp as the light source.

For rotating disc electrode (RDE) tests, the modulated speed rotator (MSR) and RDE (glassy carbon disc electrode) were purchased from Pine Co. Ltd. Catalysts (2 mg) were dispersed in ethanol (1 ml) and ultrasonically treated to obtain a homogenous catalyst ink. Then, 40 μL catalyst ink was coated on glass carbon RDE with silver conductive adhesive and dried. The linear sweep voltammetry (LSV) on the RDE was conducted in O_2 saturated $NaClO_4$ electrolyte (0.1 M, pH = 3.5) with a scan rate of 50 mV s^{-1} at rotating speeds from 0 to 2000 rpm.

2.6. Theoretical calculation

The theoretical calculation for ORR was performed using B3LYP hybrid density functional theory (DFT) coupled with 6–31 G (d) basis set provided by Gaussian 09 W. An optimized graphene cluster ($C_{35}H_{14}NS$) was used to represent SN-GQDs. The charge and spin densities for each atom were obtained from the natural population analysis (NPA) procedure. The reaction free energy ΔG was calculated according to Eq. (6) [57]:

$$\Delta G = \Delta E + \Delta ZPE - T\Delta S \quad (6)$$

wherein ΔE is the energy change between reactants and intermediates which obtained from DFT calculation, ZPE is the zero-point energy, S is the entropy, and T is the temperature setting at 298.15 K.

3. Results and discussion

3.1. Catalyst characterization

The TEM image in Fig. 1a shows that the sizes of SN-GQD/TiO_2 nanoparticles are around 20–30 nm. Many 1–2 nm black dots (partially red marked) on the surface of TiO_2 can be observed, indicating the formation of the composite of SN-GQD/TiO_2. The HR-TEM image (Fig. 1b) displays the magnified part of one nanoparticle, in which the small dots were discernible. The lattice spacing distance of 0.24 nm in a representative dot was similar to that of graphite (1120) facets [52,58], suggesting that carbon atoms in SN-GQDs have sp^2 bonded graphitic nature.

The chemical states and elemental compositions of catalysts were analyzed by XPS. The high-resolution N 1s spectrum in SN-GQD/TiO_2 (Fig. 1c) displayed two peaks at around 399.8 and 401.5 eV, which can be attributed to pyrrolic N and graphitic N or N—H bonds, respectively. These nitrogen species were also observed in N-GQD/TiO_2 (Fig. S1) and other N containing carbons [53,59–61]. The high-resolution S 2p spectrum (Fig. 1d) can be deconvoluted into two peaks, corresponding to thiophene like structure at 163.0 eV and S=O bonding at 168.3 eV, respectively. The sulfur or sulfur oxide dopants in graphene structure would induce a higher charge density to facilitate ORR [35]. These results confirmed that N and S heteroatoms were doped into the framework of GQDs.

Photoluminescence (PL) spectra of the solutions of the three GQDs under different excitation wavelengths are shown in Fig. 2. Upon excitation, the solution of GQDs showed a weak emission at around 540 nm. However, for the N-GQDs and SN-GQDs, the PL emission was centered at around 480 nm and 475 nm, respectively. Their PL intensities at the same concentrations were significantly improved, indicating that the separation efficiency of photogenerated carriers was much improved by nitrogen or/and sulfur doping. For PL spectrum of SN-GQDs, the emission wavelength shifted to 520 nm upon an excitation wavelength larger than 420 nm. The emission wavelength and intensity dependence of the excitation wavelength could be attributed to the different sizes of nanoparticles and the different emissive sites on the carbon-based materials [52]. The passivation role of N—H bonds and the synergistic S and N dual dopants, which were proved by XPS spectra, contributed to the high luminescence property of SN-GQDs.

As shown by the DRS spectra (Fig. 3a), GQDs modification made negligible changes in the optical absorption properties of TiO_2, while incorporation of N-GQDs can only induce slight visible light absorption of TiO_2. However, SN-GQD/TiO_2 displayed significant absorption in visible light region with a distinct red-shift of absorption edge from ~400 nm to more than 620 nm in comparison with bare TiO_2. This indicates the strong adsorption of SN-GQDs on TiO_2 nanoparticles. The indirect gap energy can be obtained by linearly fitting the square root of

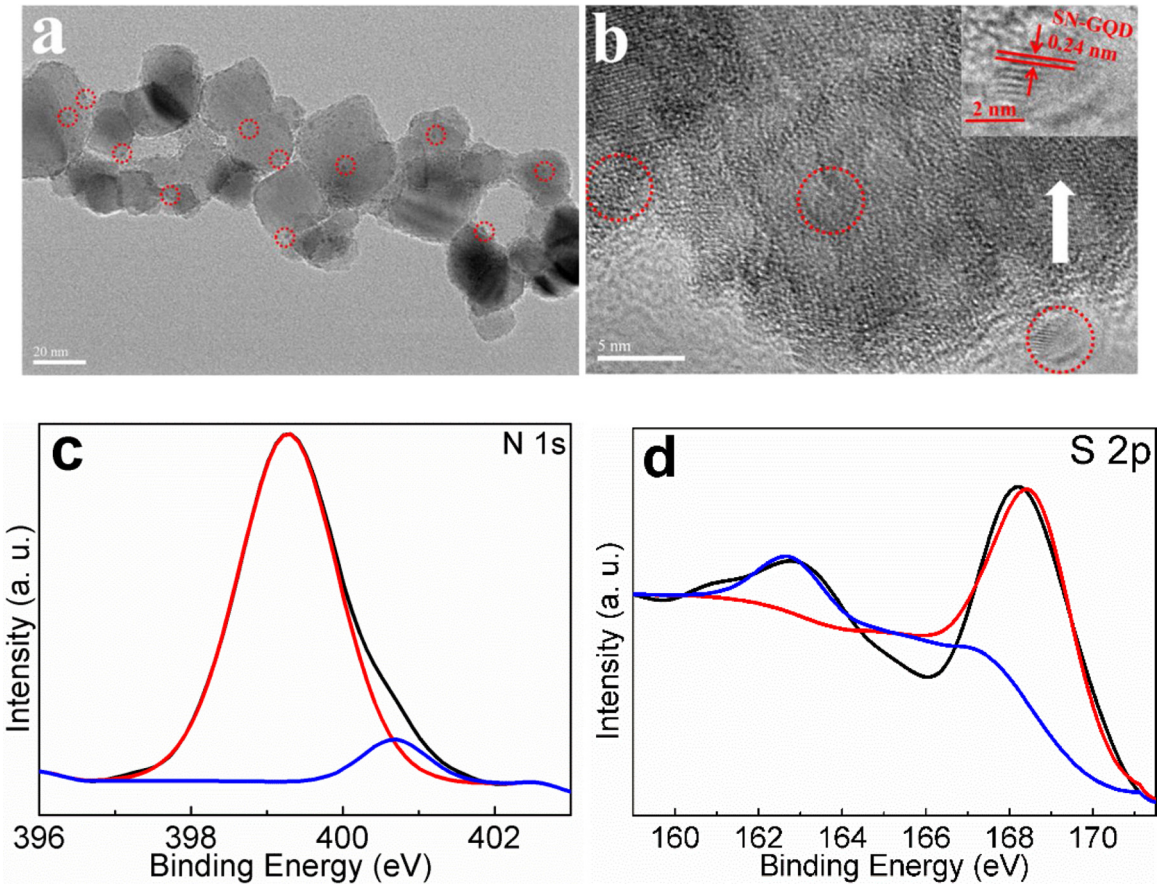

Fig. 1. (a, b) TEM images of SN-GQD/TiO_2 and (c, d) high-resolution XPS spectra (c: N 1 s and d: S 2p in SN-GQD/TiO_2).

the absorption energy against the photon energy. Notably, the band gap energy of SN-GQD/TiO_2 (1.99 eV) was obviously smaller than that of TiO_2 (3.03 eV). The narrowed band gap suggested the enhanced light-harvesting capability and improved photocatalytic activity of SN-GQD/TiO_2.

The quasi-Fermi levels of photocatalysts at any pH can be calculated based on the inflection points (pH_0) in the pH dependent photovoltage plots according to Eq. (7),

$$E_{FL}(pH) = E_0 - k(pH - pH_0) \quad (7)$$

wherein E_0 is the standard reduction potential of the redox couple (e.g. -0.45 V for MV^{2+}/MV^{+}), k is generally 0.059 V/pH for semiconductors. The E_{FL} at pH 7 were obtained as -0.57 and -0.39 V *vs.* NHE for TiO_2 and SN-GQD/TiO_2, respectively. Generally, E_{FL} corresponds to the position where electrons transfer out. The downward shift of the E_{FL} after loading of SN-GQDs indicated that electrons transferred from CB of TiO_2 to SN-GQDs, and the surface reduction mainly took place on SN-GQDs. In addition, electrochemical impedance spectra of SN-GQD/TiO_2 and TiO_2 were conducted (Fig. S2). The resistance (R_{ct}) for charge transfer through the solid/liquid interface correlates with the semicircle diameter at high frequencies. The SN-GQD/TiO_2 electrode displayed a lower R_{ct} than TiO_2, indicating an enhancement of charge separation in the excited SN-GQD/TiO_2. The enhanced electron migration after loading of SN-GQDs can retard electron-hole recombination and favor photocatalytic performance.

3.2. Photocatalytic activity for H_2O_2 production

As shown in Fig. 4, one can see that the production of H_2O_2 in SN-GQD/Al_2O_3 suspensions under both visible light and simulated sunlight sources is negligible. This indicates that SN-GQDs solely possesses a poor photocatalytic activity for O_2 reduction. Bare TiO_2 also showed a low activity in H_2O_2 production, namely, only 140 μM H_2O_2 was detected after illumination by simulated sunlight for 60 min. The undoped or doped GQDs modified TiO_2 exhibited enhanced production of H_2O_2, which is dependent on their dosages (Fig. S3). The optimized dosages for GQDs, N-GQDs and SN-GQDs were 1.0, 0.3, and 0.5%, respectively. The production of H_2O_2 on these modified TiO_2 catalysts firstly increased with the increase of GQDs content due to their favorable effects on enhancing photocatalytic activity. However, excess surface modifier would cover some active adsorption sites and decrease the accessibility of oxygen and hole scavengers, resulting in a reduction of H_2O_2 production. The composites with optimal dosages of GQDs were deeply evaluated in the following discussion.

Under visible light irradiation (Fig. 4a), GQDs and N-GQDs modified TiO_2 showed slightly enhanced photocatalytic activity in H_2O_2 production. However, SN-GQDs modification significantly improved the production of H_2O_2, namely, more than 82.8 μM H_2O_2 was produced after 90 min irradiation. This is around 5.3 and 3.1 times of the corresponding value in the GQD/TiO_2 and N-GQD/TiO_2 suspensions, respectively. The visible light activity of these composites can be mainly attributed to the sensitization of GQDs, which can absorb visible light and induce electron excitation and separation [39,52]. The highest visible light photocatalytic activity of SN-GQD/TiO_2 is in accordance with its wide optical absorption range and highest luminescence performance. Under simulated sunlight irradiation (Fig. 4b), N-GQDs and SN-GQDs modifications obviously promoted photocatalytic activity, leading to 339 and 451 μM of H_2O_2 at 60 min, respectively, which are 2.4 and 3.2 folds as that for bare TiO_2. Therefore, SN-GQD/TiO_2 displayed highest photocatalytic activity for H_2O_2 production under both light sources.

The photocatalytic degradation of H_2O_2 on catalysts were shown in

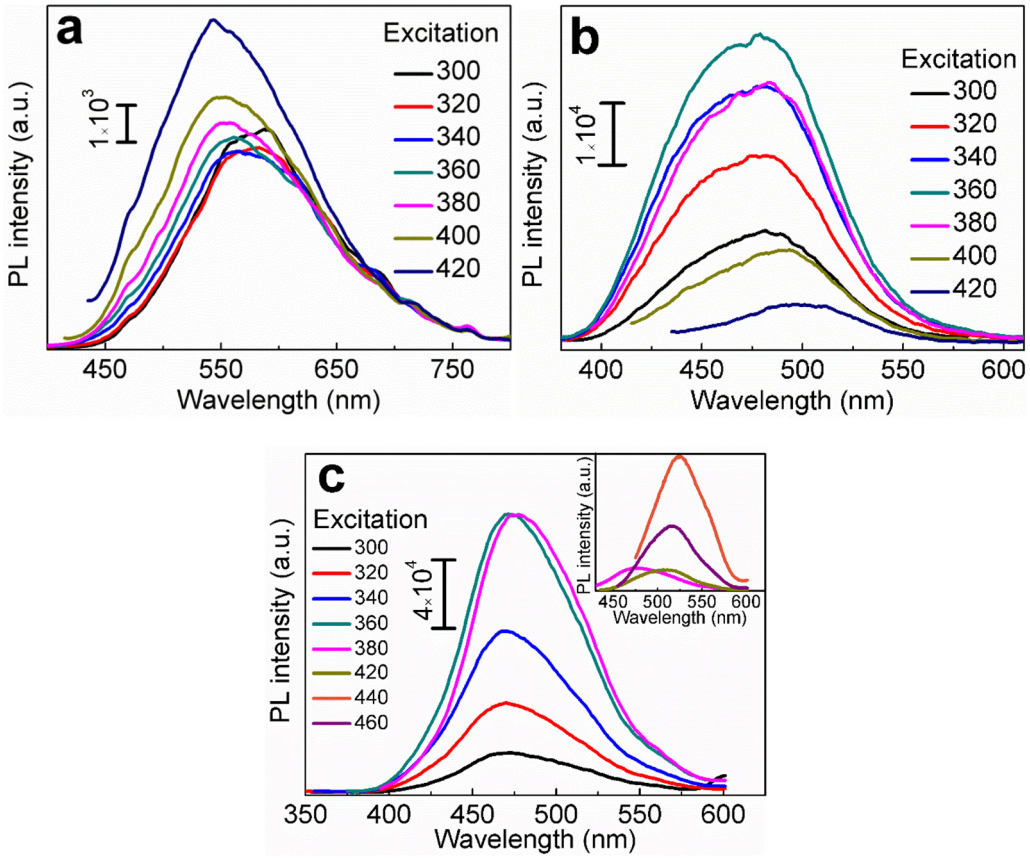

Fig. 2. Photoluminescence spectra of (a) GQD/TiO_2, (b) N-GQD/TiO_2 and (c) SN-GQD/TiO_2.

Fig. 4c and d. Under visible light illumination, bare TiO_2 exhibited a high H_2O_2 decomposition rate (0.023 min^{-1}) due to the formation of visible light responsive Ti—OOH groups on the surface. After surface modification, H_2O_2 decomposition under visible light irradiation was significantly suppressed. The photocatalytic degradation of H_2O_2 on SN-GQD/TiO_2 decreased to as low as 0.005 min^{-1}. However, under simulated sunlight, surface modification can only moderately inhibit H_2O_2 decomposed, whose rates moderately decreased from 0.098 min^{-1} for bare TiO_2 to the lowest 0.074 min^{-1} for SN-GQD/TiO_2, achieving about 25% reduction. This suggests that surface modification of GQDs would inhibit the charge transfer from the $\equiv Ti - OOH$ groups toward CB of TiO_2 under visible light irradiation, but could only partially suppress the formation of the surface complexes. The decreased H_2O_2 decomposition rate for SN-GQD/TiO_2 was mainly attributed to the less complexes of $\equiv Ti - OOH$ formed on the surface of TiO_2 due to decreased exposed surface after SN-GQDs modification. Besides H_2O_2, the photogenerated holes could also be competitively consumed by hole scavengers (like isopropanol) or surface hydroxyl groups [62,63].

The kinetics of H_2O_2 production can be evaluated according to the formation and decomposition rates of H_2O_2. In oxygen saturated solution, the formation rate is determined by zero-order kinetics and the decomposition rate by the first-order kinetics. Therefore, the H_2O_2 concentration in illuminated suspensions can be calculated by Eq. (8) [9,14], where k_f and k_d are the H_2O_2 formation

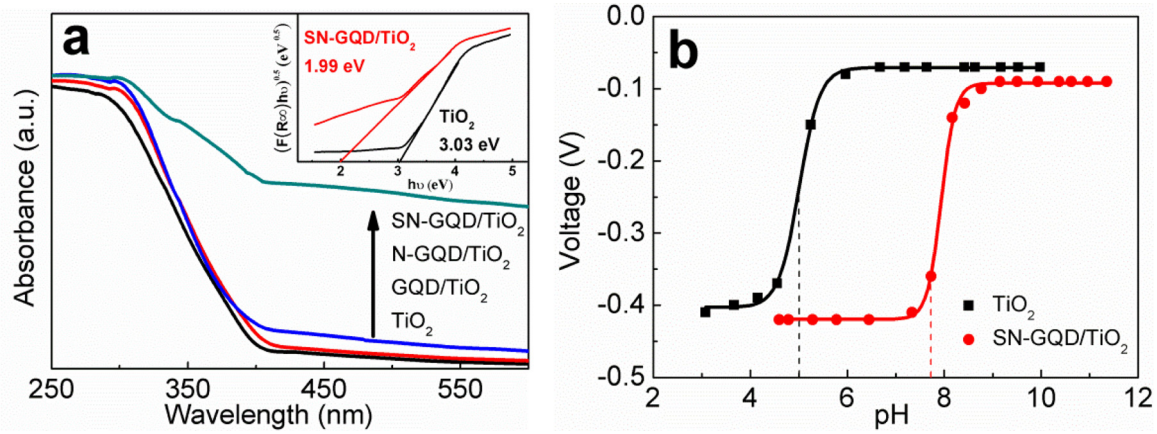

Fig. 3. (a) UV–vis diffuse reflectance spectra (DRS) of TiO_2 and the three GQDs modified TiO_2, inset: Plots of $(F(R_\infty)h\nu)^{0.5}$ *vs.* the energy of absorbed light for TiO_2 and SN-GQD/TiO_2; (b) Photovoltage *vs.* suspension pH value measured for TiO_2 and SN-GQD/TiO_2 in the presence of MV^{2+}.

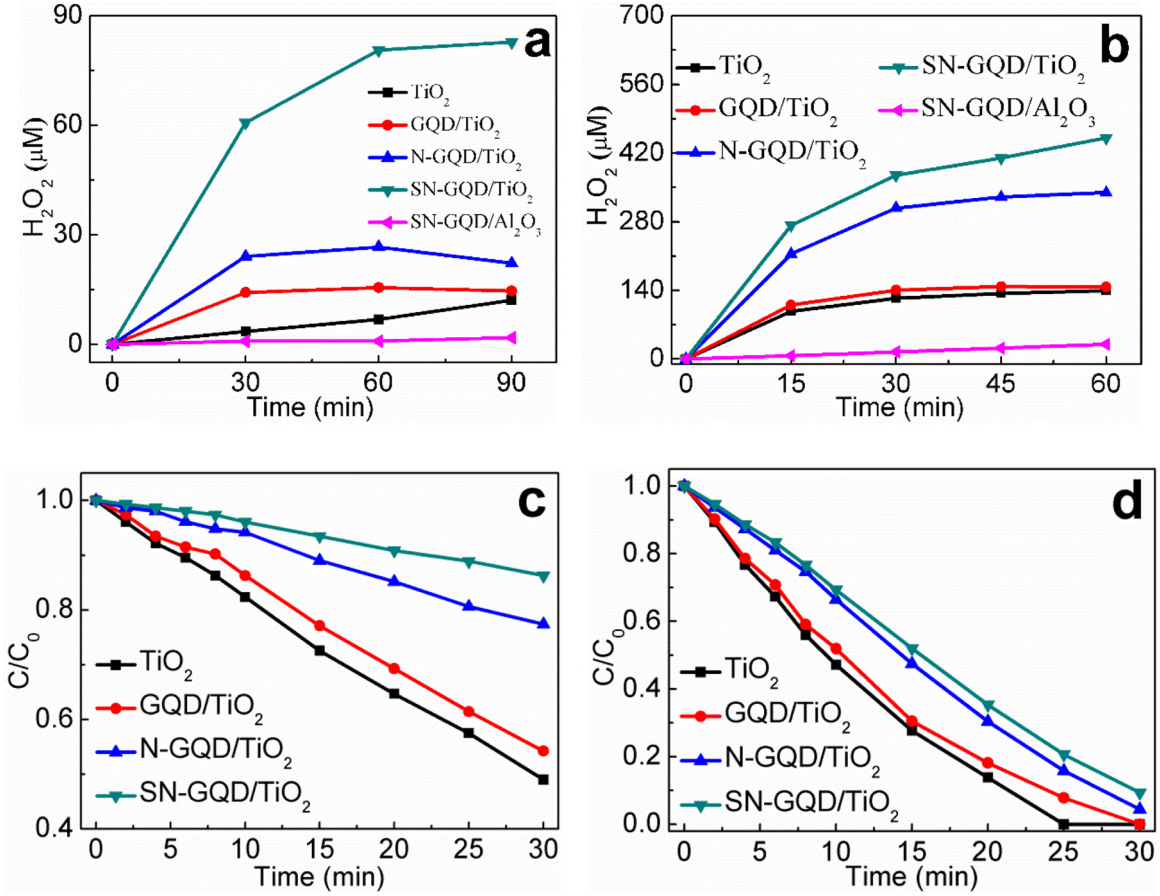

Fig. 4. Photocatalytic generation of H_2O_2 (a, b) and photocatalytic degradation of H_2O_2 (c, d) on various catalysts under visible light (a, c) and simulated sunlight (b, d) irradiation.

$$[H_2O_2] = (k_f/k_d)\,[1 - \exp(-k_d t)] \quad (8)$$

and decomposition rate constants, respectively. The production of H_2O_2 is positively related to k_f and inversely proportional to k_d. We measured k_d values and estimated k_f values according to Eq. (8), and the rate constants were compared in Fig. 5a and b. Bare TiO_2 exhibited the relatively larger k_d and lower k_f, leading to the worst production of H_2O_2. Surface modification of TiO_2 by various GQDs increased k_f but decreased k_d values. Furthermore, SN-GQD/TiO_2 exhibited the lowest k_d value, about 75% of that for bare TiO_2 under simulated sunlight. The decreased efficiency for H_2O_2 decomposition on modified TiO_2 was not consistent to their enhanced photocatalytic activities for phenol degradation (Fig. S4). This can be attributed to that the decomposition of H_2O_2 was governed by adsorption, which was suppressed by surface SN-GQDs modification, whereas phenol was mainly degraded by free radicals [64,65]. In addition to the inhibited decomposition of H_2O_2, all the three GQDs modifications promoted the formation of H_2O_2; among them, the SN-GQD/TiO_2 had the highest k_f values, which was around 2.4 times of that for TiO_2 under simulated sunlight. The overall high H_2O_2 production in the SN-GQD/TiO_2 suspension was attributed to the enhanced formation and the inhibited decomposition of H_2O_2. However, considering the moderate decrease of decomposition rate in comparison to bare TiO_2, the contribution from the accelerated formation rates was predominated.

Photocatalytic degradation of phenol (Fig. S4) and photocurrent

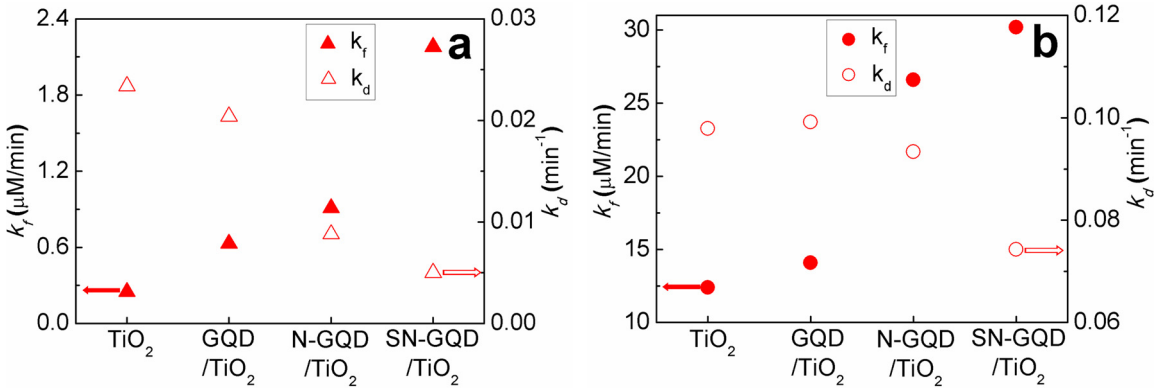

Fig. 5. The formation rate constants (k_f, filled symbol) and decomposition rate constants (k_d, open symbol) of H_2O_2 for various catalysts under (a) visible light and (b) simulated sunlight irradiation.

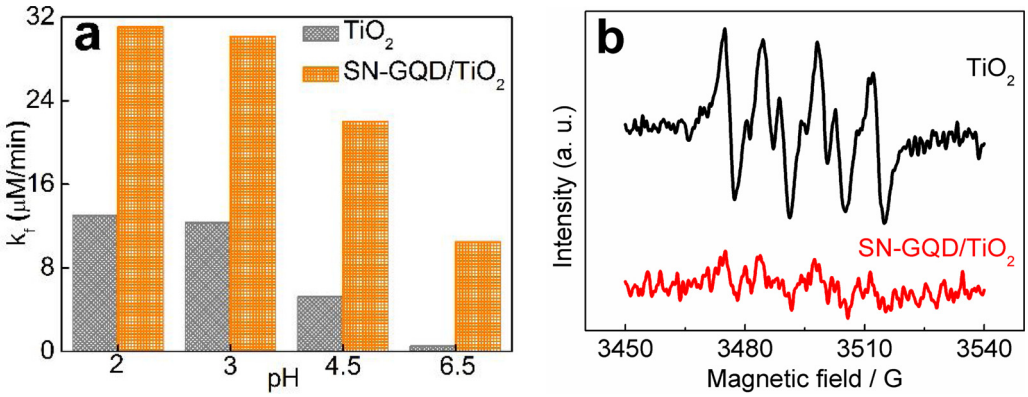

Fig. 6. (a) The H_2O_2 formation rate constants (k_f) at different pHs; (b) ESR spectra of TiO_2 and SN-GQD/TiO_2 systems after 25 min illumination.

generation (Fig. S5) were carried out to evaluate the photocatalytic activity of SN-GQD/TiO_2. Under simulate sunlight, degradation rate constants of phenol on bare TiO_2 and SN-GQD/TiO_2 were 0.0185 and 0.0208 min^{-1}, respectively; and their photocurrent densities were 70 and 94 μA/cm^2, respctively. The enhancement factors after SN-GQDs modification were only 1.1 and 1.3 for phenol degradation and photocurrent generation, respectively. Comparing to GQDs and N-GQDs, the codoped N and S atoms in SN-GQDs could act as an electron donor to increase the concentration of charge carriers and enhance the conductivity of carbon matrix [34,66,67]. Therefore, loading of SN-GQDs resulted in a better enhancement in electron migration. However, the enhancement factors were much lower than those for production and formation of H_2O_2 in the SN-GQD/TiO_2 suspension. This indicates that there might be other-even more crucial-reasons to boost H_2O_2 production in addition to the above mentioned favorable effects.

The effect of proton concentrations on H_2O_2 formation and decomposition are shown in Fig. 6a and Fig. S6, resepctively. The k_f decreased while k_d increased as the pH value increased for both of catalysts. The highly pH dependent H_2O_2 production indicated that the formation of H_2O_2 was governed by the proton-coupled electron transfer (PCET) mechanism [14,68]. The accelerated H_2O_2 photodecomposition with the increase of pH could be attributed to the enhanced adsorption of H_2O_2 on the surface of TiO_2 [32]. Moreover, H_2O_2 production in the SN-GQD/TiO_2 suspension was less sensitive to proton concentration. At pH 6.5, the k_f value for SN-GQD/TiO_2 was 10.5 μM/min, and about 112 μM H_2O_2 was produced after 60 min irradiation; while negligible H_2O_2 can be measured in the TiO_2 suspension. This suggested that the ORR for H_2O_2 production on SN-GQD/TiO_2 did not require high acidic conditions to stabilize superoxide radicals, a typical intermediate in the one-electron ORR pathway. The suppressed generation of superoxide radicals was confirmed by ESR spectra (Fig. 6b). The typical signals of DMPO–$O_2\cdot^-$ were significant in the TiO_2 suspension after 25 min illumination under simulated sunlight, while such signals were barely identifiable in the illuminated SN-GQD/TiO_2 system. The suppressed generation of the typical intermediate of $O_2\cdot^-$ indicated a less possible one-electron ORR pathway.

3.3. Two-electron ORR pathway

Linear sweep voltammogram (LSV) on a rotating disc electrode (RDE) was recorded to gain insight about the oxygen reduction reaction (ORR) and H_2O_2 production on the dual doped CQDs tuned TiO_2. Fig. 7a shows LSV curves of various electrodes without rotation in oxygen saturated electrolytes, in which the cathodic current density represents the ORR rates on the surface of photocatalysts. The three GQDs modified TiO_2 catalysts showed higher cathodic current densities than TiO_2, indicating that modification of GQDs can promote ORR on TiO_2. The ORR current of SN-GQD/TiO_2 is explicitly higher than that of GQD/TiO_2 and N-GQD/TiO_2 over the whole potential range, which is about 2.4 times of the bare TiO_2 at −0.8 V *vs.* Ag/AgCl, suggesting that the synergistic effect of dual S and N doping GQDs facilitated electrons transfer from TiO_2 to O_2 and enhanced ORR rates.

Fig. 7b and Fig. S7 displays the LSV on various electrodes at rotation speeds from 0 to 2000 rpm in the O_2 saturated electrolytes. The cathodic current density increased with increasing rotation speed. The relationship between current density and rotation speed at plateau currents was described by Koutecky-Levuch equation (Fig. 7c). The overall number of the transferred electrons (n) and the kinetic current density (i_k) in ORR were quantitatively estimated according to the slope and intercept of the linearly fitted plots [69], respectively (Fig. 7d). All corresponding Koutecky–Levich (K–L) plots exhibited good linearity (Fig. 7c). The n values were 1.3 for both bare TiO_2 and GQD/TiO_2, indicating that ORR on both catalysts was dominated by a one-electron process, and undoped GQDs modification cannot alter the ORR pathway. However, the i_k value increased by 64% after GQDs modification, indicating that the kinetic rate of ORR was accelerated by GQDs. This could be attributed to the facilitated charge transfer. The n values of N-GQD/TiO_2 and SN-GQD/TiO_2 electrodes increased to 1.6 and 2.2, respectively. Therefore, ORR on N-GQD/TiO_2 was a mixture of one-electron and two-electron pathways, while that on SN-GQD/TiO_2 was dominated by a two-electron pathway. Simultaneously, the i_k values dramatically increased from 5.9 mA cm^{-2} (bare TiO_2) to 86 mA cm^{-2} (SN-GQD/TiO_2) at −0.75 V *vs.* Ag/AgCl, which was nearly 9 and 2 times higher than those of GQD/TiO_2 and N-GQD/TiO_2, respectively. The significantly high i_k value and the two-electron ORR pathway rationalized the high selectivity in photocatalytic H_2O_2 formation and production on SN-GQD/TiO_2 [18,70].

The effect of dual N and S doping in GQDs were previously recognized in ORR and other catalysis [34,71,72]. According to DFT calculations (Scheme 1), the S and N changed the charge density or spin density of carbon atoms of graphene [34,72]. The more electronegative N atoms (3.04 eV *vs.* 2.55 eV and 2.58 eV for respective carbon and sulfur) induce electron transfer out from the neighboring C atoms and lead to a high positive charge density on the adjacent C atoms (C1, C2, and C3 in Scheme 1). Introduction of S atoms into the N-doped graphene can further increase the charge density of those C atoms adjacent to N dopants, while simultaneously induce negative charge density to those adjacent to S atoms (C4 and C5 in Scheme 1). The carbon and sulfur atoms with positive charge density can serve as potential active sites for ORR by increasing molecular oxygen adsorption; while those carbon and nitrogen atoms with negative charge density can play as the proton relay sites to enhance the PCET processes in multi-electron ORR.

The rearrangement of electronic distribution in the SN-GQDs (Scheme 1 a) provides the requirements for two-electron ORR in the photocatalysis of SN-GQD/TiO_2. Firstly, molecular oxygen is adsorbed on the surface of SN-GQDs due to the high affinity of oxygen toward those atoms that have a positive charge density (Scheme 1 b and c).

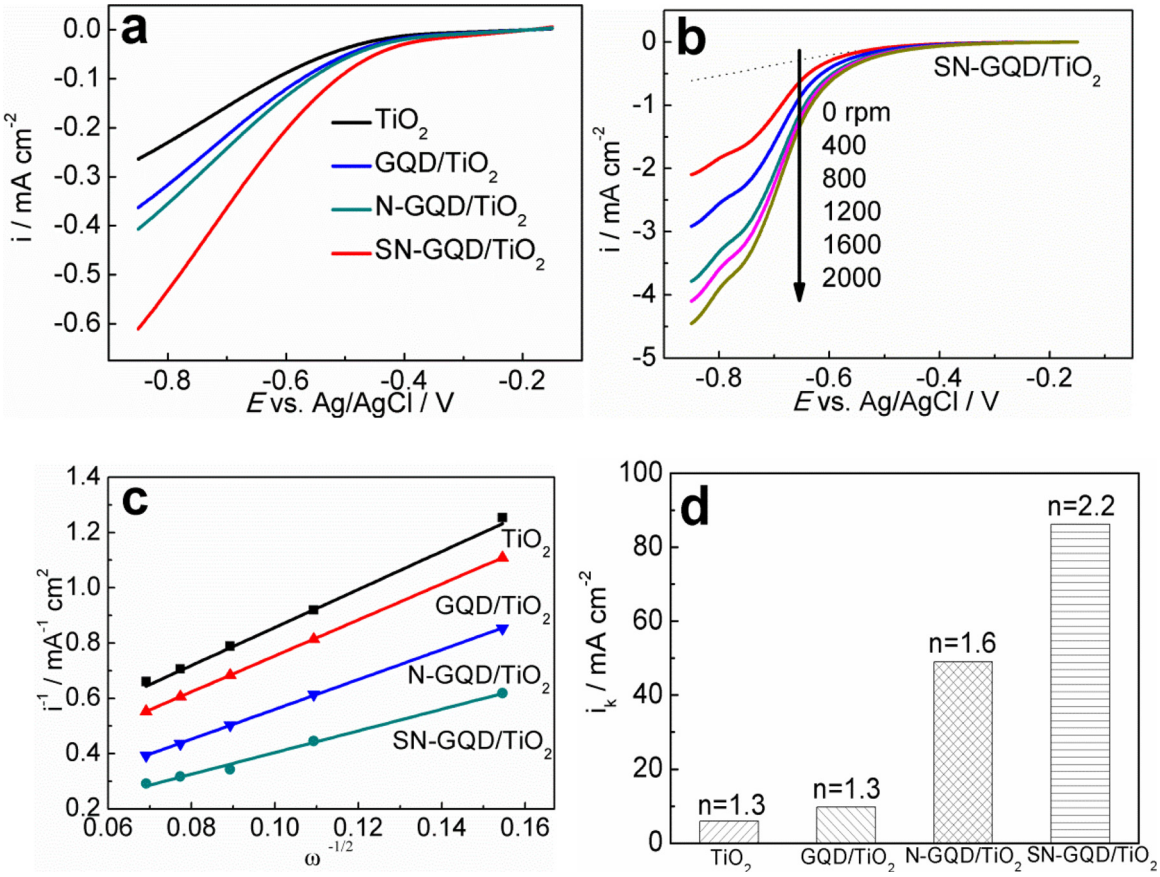

Fig. 7. (a) Linear sweep voltammetry (LSV) of TiO_2, GQD/TiO_2, N-GQD/TiO_2 and SN-GQD/TiO_2 film electrodes in O_2-saturated 0.1 M $NaClO_4$ (pH = 3.5, 50 mV s^{-1}) without rotation; (b) LSV of SN-GQD/TiO_2 film electrode in O_2-saturated 0.1 M $NaClO_4$ at different rotating speeds; (c) Koutecky-Levuch plots of bare TiO_2 and SN-GQD/TiO_2 films at −0.75 V *vs.* Ag/AgCl; (d) Kinetic limiting current density (i_k) of different samples as well as the corresponding electron-transfer numbers at −0.75 V *vs.* Ag/AgCl.

Then, upon illumination, electrons and holes generated from excited TiO_2 nanoparticles could be trapped by SN-GQDs and alcohol molecules, respectively. One electron on SN-GQDs is captured by the adsorbed oxygen to promote formation of OOH groups on the S atom, which had the largest positive charge density. The existence of hydroperoxo intermediates on the illuminated SN-GQD/TiO_2 was confirmed by Raman spectroscopy (Fig. S8). A new band appeared at 866 cm^{-1} in the illuminated SN-GQD/TiO_2, which corresponded to the O—O vibration in the hydroperoxo groups (OOH) [73]. Due to the relative stable of the hydroperoxo species, it is less possible to produce free superoxide radicals. This was confirmed by ESR spectra in Fig. 6b. Simultaneously, photogenerated holes (h^+) oxidize alcohol by removing the α- and β-hydrogens and producing aldehyde or ketone and protons. The C (C4, C5) and N sites possessing negative charge density offer active sites to capture protons (Scheme 1 d). Finally, the *OOH species are readily transformed into H_2O_2 by combining with another electron and proton, and then SN-GQDs are ready for next H_2O_2 production cycle. The adsorption of OOH species on SN-GQDs and the presence of proton relay

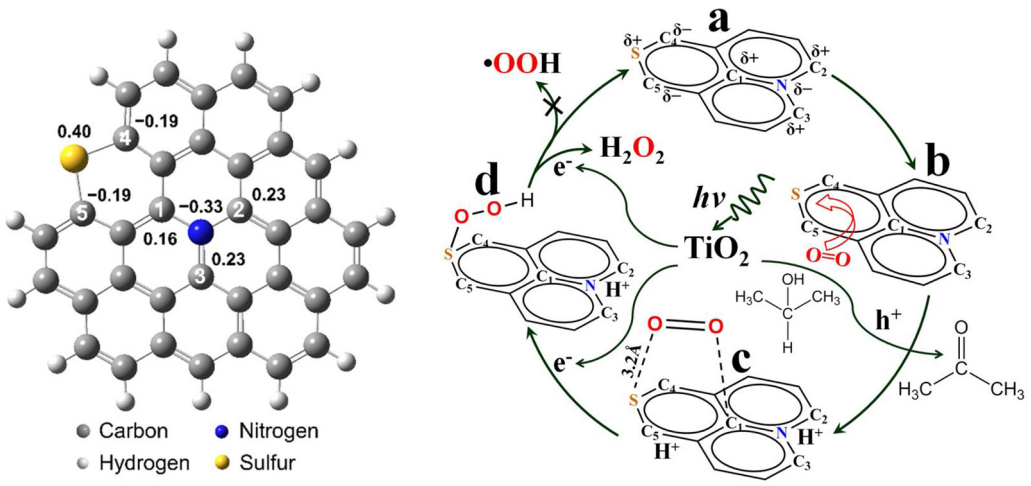

Scheme 1. Proposed mechanism for H_2O_2 formation on the photoactivated SN-GQD/TiO_2.

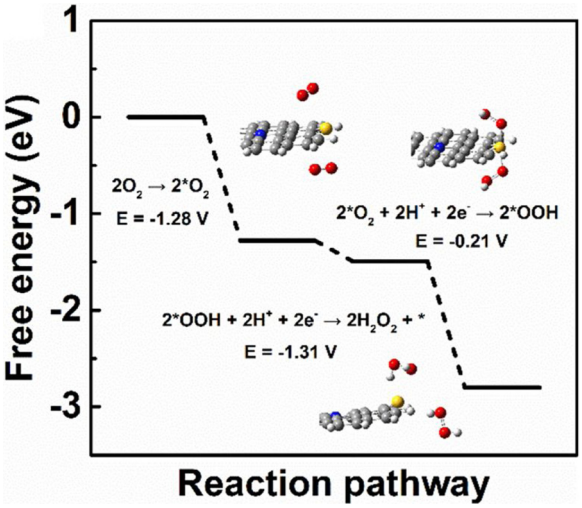

Fig. 8. Free energy diagrams of ORR reaction pathways on SN-GQDs active sites (*). The inset is the reaction intermediates.

sites in SN-GQDs significantly promotes selective two-electron ORR and increases the production of H_2O_2 on SN-GQD/TiO_2.

To gain a fundamental knowledge on the mechanism, the free energy diagram for each step in the ORR on SN-GQDs was obtained based on DFT calculations (Fig. 8). Two O_2 molecules were firstly adsorbed on the SN-GQDs with thermodynamically downslope of −1.28 eV. The O—O bonds stretching were not significant (< 0.02 Å), thus they were not easily broken. Then, the adsorbed O_2 was quickly transformed to *OOH by coupling a proton and an electron due to the tiny energy downslope. The two OOH species could adsorb on S atom with a distance of 1.87 Å, indicating the formation of S—O covalent bonds [35]. Finally, two more protons and electrons were introduced to produce two H_2O_2 molecules, which are desorbed from the SN-GQDs with a distance of 3.3 Å after optimization. The reaction free energy in this step was −1.31 eV, indicating that the H_2O_2 overall evolution was spontaneously favorable. These results were well consistent with the proposed mechanism described in Scheme 1, demonstrating the vital role of SN-GQDs in the high selectivity of the two-electron ORR pathway.

4. Conclusions

In summary, sulfur and nitrogen dual doped GQDs can dramatically enhance H_2O_2 production on TiO_2 under both visible light and simulated sunlight irradiation. The enhanced performance is attributed to the boosted two-electron ORR that mainly takes place on the surface modifier (SN-GQDs). The mechanism on the fast generation of *OOH and subsequent reduction to H_2O_2 on SN-GQDs is proposed to understand the highly selective two-electron reduction of oxygen. It can be expected that H_2O_2 production can be further improved by the incorporation of approaches to suppress H_2O_2 decomposition. This study demonstrated a promising strategy to realize highly selective two-electron ORR for efficient photocatalytic H_2O_2 production by tuning TiO_2 with carbon materials that can provide two active sites.

Acknowledgements

Financial supports from the Special Fund for Agro–scientific Research in the Public Interest (201503107) and the Natural Science Foundation of China (21876108, 21377084) are gratefully acknowledged. The helps on theoretical calculations from Chunyang Yu of School of Chemistry and Chemical Engineering, Shanghai Jiao Tong University and Lidong Gong of School of Chemistry and Chemical Engineering, Liaoning Normal University are gratefully acknowledged. We also acknowledge the valuable suggestion in PL and XPS analyses from Ms. Xiaofang Hu of School of Environmental Science and Engineering and Dr. Limin Sun of the Instrumental Analysis Center of Shanghai Jiao Tong University.

Appendix A. Supplementary data

Supplementary material related to this article can be found, in the online version, at doi:https://doi.org/10.1016/j.apcatb.2018.08.031.

References

[1] J.M. Campos-Martin, G. Blanco-Brieva, J.L. Fierro, Hydrogen peroxide synthesis: an outlook beyond the anthraquinone process, Angew. Chem. In. Ed. 45 (2006) 6962–6984.
[2] S. Kang, L. Zhang, C. Liu, L. Huang, H. Shi, L. Cui, Hydrogen peroxide activated commercial P25 TiO_2 as efficient visible-light-driven photocatalyst on dye degradation, Int. J. Electrochem. Sci. 12 (2017) 5284–5293.
[3] L.S. Walekar, P. Hu, F. Liao, X. Guo, M. Long, Turn-on fluorometric and colorimetric probe for hydrogen peroxide based on the in-situ formation of silver ions from a composite made from N-doped carbon quantum dots and silver nanoparticles, Microchim. Acta 185 (2018) 31–39.
[4] A. Asghar, A.A. Abdul Raman, W.M.A. Wan Daud, Advanced oxidation processes for in-situ production of hydrogen peroxide/hydroxyl radical for textile wastewater treatment: a review, J. Clean. Prod. 87 (2015) 826–838.
[5] Z. Zheng, Y.H. Ng, D.W. Wang, R. Amal, Epitaxial growth of Au-Pt-Ni nanorods for direct high selectivity H_2O_2production, Adv. Mater. 28 (2016) 9949–9955.
[6] S.J. Freakley, Q. He, J.H. Harrhy, L. Lu, D.A. Crole, D.J. Morgan, E.N. Ntainjua, J.K. Edwards, A.F. Carley, A.Y. Borisevich, C.J. Kiely, G.J. Hutchings, Palladium-tin catalysts for the direct synthesis of H_2O_2 with high selectivity, Science 351 (2016) 965–968.
[7] R. Dittmeyer, J.D. Grunwaldt, A. Pashkova, A review of catalyst performance and novel reaction Engineering concepts in direct synthesis of hydrogen peroxide, Catal. Today 248 (2015) 149–159.
[8] A.J. Hoffman, E.R. Carraway, M.R. Hoffmann, Photocatalytic production of H_2O_2 and organic peroxides on quantum-sized semiconductor collolds, Environ. Sci. Technol. 28 (1994) 776–785.
[9] C. Kormann, D.W. Bahnemann, M.R. Hoffmann, Photocatalytic production of H_2O_2 and organic peroxides in aqueous suspensions of TiO_2, ZnO, and desert Sand, Environ. Sci. Technol. 22 (1988) 798–806.
[10] R. Cai, Y. Kubota, A. Fujishima, Effect of copper ions on the formation of hydrogen peroxide from photocatalytic titanium dioxide particles, J. Catal. 219 (2003) 214–218.
[11] V. Maurino, C. Minero, G. Mariella, E. Pelizzetti, Sustained production of H_2O_2 on irradiated TiO_2-fluoride systems, Chem. Commun. 20 (2005) 2627–2629.
[12] V. Maurino, C. Minero, E. Pelizzetti, G. Mariella, A. Arbezzano, F. Rubertelli, Influence of Zn(II) adsorption on the photocatalytic activity and the production of H_2O_2 over irradiated TiO_2, Res. Chem. Intermed. 33 (2007) 319–332.
[13] D. Tsukamoto, A. Shiro, Y. Shiraishi, Y. Sugano, S. Ichikawa, S. Tanaka, T. Hirai, Photocatalytic H_2O_2 production from ethanol/O_2 system using TiO_2 loaded with Au-Ag bimetallic alloy nanoparticles, ACS Catal. 2 (2012) 599–603.
[14] G.-H. Moon, W. Kim, A.D. Bokare, N.-E. Sung, W. Choi, Solar production of H_2O_2 on reduced graphene oxide-TiO_2 hybrid photocatalysts consisting of earth-abundant elements only, Energy Environ. Sci. 7 (2014) 4023–4028.
[15] Y. Shiraishi, S. Kanazawa, Y. Kofuji, H. Sakamoto, S. Ichikawa, S. Tanaka, T. Hirai, Sunlight-driven hydrogen peroxide production from water and molecular oxygen by metal-free photocatalysts, Angew. Chem. In. Ed. 53 (2014) 13454–13459.
[16] Y. Shiraishi, S. Kanazawa, Y. Sugano, D. Tsukamoto, H. Sakamoto, S. Ichikawa, T. Hirai, Highly selective production of hydrogen peroxide on graphitic carbon nitride (g-C_3N_4) photocatalyst activated by visible light, ACS Catal. 4 (2014) 774–780.
[17] J.R. Harbour, J. Tromp, M.L. Hair, Photogeneration of hydrogen peroxide in aqueous TiO_2 dispersions, Can. J. Chem. 63 (1985) 204–208.
[18] H. Sheng, H. Ji, W. Ma, C. Chen, J. Zhao, Direct four-electron reduction of O_2 to H_2O on TiO_2 surfaces by pendant proton relay, Angew. Chem. In. Ed. 52 (2013) 9686–9690.
[19] S. Li, G. Dong, R. Hailili, L. Yang, Y. Li, F. Wang, Y. Zeng, C. Wang, Effective photocatalytic H_2O_2 production under visible light irradiation at g-C_3N_4 modulated by carbon vacancies, Appl. Catal. B: Environ. 190 (2016) 26–35.
[20] Y. Shiraishi, Y. Kofuji, H. Sakamoto, S. Tanaka, S. Ichikawa, T. Hirai, Effects of surface defects on photocatalytic H_2O_2 production by mesoporous graphitic carbon nitride under visible light irradiation, ACS Catal. 5 (2015) 3058–3066.
[21] L. Yang, G. Dong, D.L. Jacobs, Y. Wang, L. Zang, C. Wang, Two-channel photocatalytic production of H_2O_2 over g-C_3N_4 nanosheets modified with perylene imides, J. Catal. 352 (2017) 274–281.
[22] M. Long, L. Zheng, Engineering vacancies for solar photocatalytic applications, Chin. J. Catal. 38 (2017) 617–624.
[23] H. Hirakawa, S. Shiota, Y. Shiraishi, H. Sakamoto, S. Ichikawa, T. Hirai, Au nanoparticles supported on $BiVO_4$: effective inorganic photocatalysts for H_2O_2 production from water and O_2 under visible light, ACS Catal. 6 (2016) 4976–4982.
[24] K. Mase, M. Yoneda, Y. Yamada, S. Fukuzumi, Efficient photocatalytic production of hydrogen Peroxide from water and dioxygen with bismuth vanadate and a cobalt

(II) chlorin complex, ACS Energy Lett. 1 (2016) 913–919.
[25] K. Fuku, Y. Miyase, Y. Miseki, T. Funaki, T. Gunji, K. Sayama, Photoelectrochemical hydrogen peroxide production from water on a WO_3/$BiVO_4$photoanode and from O_2 on an Au cathode without external bias, Chem. Asian J. 12 (2017) 1111–1119.
[26] H. Zhuang, L. Yang, J. Xu, F. Li, Z. Zhang, H. Lin, J. Long, X. Wang, Robust photocatalytic H_2O_2 production by octahedral $Cd_3(C_3N_3S_3)_2$ coordination polymer under visible light, Sci. Rep. 5 (2015) 16947–16957.
[27] J. Xu, Z. Chen, H. Zhang, G. Lin, H. Lin, X. Wang, J. Long, $Cd_3(C_3N_3S_3)_2$ coordination polymer/graphene nanoarchitectures for enhanced photocatalytic H_2O_2 production under visible light, Sci. Bull. 62 (2017) 610–618.
[28] S. Thakur, T. Kshetri, N.H. Kim, J.H. Lee, Sunlight-driven sustainable production of hydrogen peroxide using a CdS-graphene hybrid photocatalyst, J. Catal. 345 (2017) 78–86.
[29] H.I. Kim, O.S. Kwon, S. Kim, W. Choi, J.H. Kim, Harnessing low energy photons (635 nm) for the production of H_2O_2 using upconversion nanohybrid photocatalysts, Energy Environ. Sci. 9 (2016) 1063–1073.
[30] S. Gogoi, N. Karak, Solar-driven hydrogen peroxide production using polymer-supported carbon dots as heterogeneous catalyst, Nano-Micro Lett. 9 (2017) 40.
[31] L. Kong, X. Zhang, C. Wang, F. Wan, L. Li, Synergic effects of Cu_xO electron transfer co-catalyst and valence band edge control over TiO_2 for efficient visible-light photocatalysis, Chin. J. Catal. 38 (2017) 2120–2131.
[32] X.Z. Li, C.C. Chen, J.C. Zhao, Mechanism of photodecomposition of H_2O_2 on TiO_2 surfaces under visible light irradiation, Langmuir 17 (2001) 4118–4122.
[33] L. Zheng, X. Yu, M. Long, Q. Li, Humic acid-mediated visible-light degradation of phenol on phosphate-modified and nafion-modified TiO_2 surfaces, Chin. J. Catal. 38 (2017) 2076–2084.
[34] J. Liang, Y. Jiao, M. Jaroniec, S.Z. Qiao, Sulfur and nitrogen dual-doped mesoporous graphene electrocatalyst for oxygen reduction with synergistically enhanced performance, Angew. Chem. In. Ed. 51 (2012) 11496–11500.
[35] L. Zhang, J. Niu, M. Li, Z. Xia, Catalytic mechanisms of sulfur-doped graphene as efficient oxygen reduction reaction catalysts for fuel cells, J. Phys. Chem. C 118 (2014) 3545–3553.
[36] X. Sun, Y. Zhang, P. Song, J. Pan, L. Zhuang, W. Xu, W. Xing, Metal nanoparticle/carbon quantum dot composite as a photocatalyst for high-efficiency cyclohexane oxidation, ACS Catal. 3 (2013) 1726–1729.
[37] M. Long, Y. Qin, C. Chen, X. Guo, B. Tan, W. Cai, Origin of visible light photoactivity of reduced graphene oxide/TiO_2 by in situ hydrothermal growth of undergrown TiO_2 with graphene oxide, J. Phys. Chem. C 117 (2013) 16734–16741.
[38] J. Kong, W. Cheng, Recent advances in the rational design of electrocatalysts towards the oxygen reduction reaction, Chin. J. Catal. 38 (2017) 951–969.
[39] G. Xie, K. Zhang, B. Guo, Q. Liu, L. Fang, J.R. Gong, Graphene-based materials for hydrogen generation from light-driven water splitting, Adv. Mater. 25 (2013) 3820–3839.
[40] N. Zhang, M.Q. Yang, S. Liu, Y. Sun, Y.J. Xu, Waltzing with the versatile platform of graphene to synthesize composite photocatalysts, Chem. Rev. 115 (2015) 10307–10377.
[41] B. Weng, J. Wu, N. Zhang, Y.J. Xu, Observing the role of graphene in boosting the two-electron reduction of oxygen in graphene-WO_3 nanorod photocatalysts, Langmuir 30 (2014) 5574–5584.
[42] C. Wang, M. Long, B. Tan, L. Zheng, J. Cai, J. Fu, Facilitated photoinduced electron storage and two-electron reduction of oxygen by reduced graphene oxide in rGO/TiO_2/WO_3 composites, Electrochim. Acta 250 (2017) 108–116.
[43] A. Qu, H. Xie, X. Xu, Y. Zhang, S. Wen, Y. Cui, High quantum yield graphene quantum dots decorated TiO_2 nanotubes for enhancing photocatalytic activity, Appl. Surf. Sci. 375 (2016) 230–241.
[44] Q. Mei, K. Zhang, G. Guan, B. Liu, S. Wang, Z. Zhang, Highly efficient photoluminescent graphene oxide with tunable surface properties, Chem. Commun. 46 (2010) 7319–7321.
[45] X.T. Zheng, A. Ananthanarayanan, K.Q. Luo, P. Chen, Glowing graphene quantum dots and carbon dots: properties, syntheses, and biological applications, Small 11 (2015) 1620–1636.
[46] H. Tetsuka, R. Asahi, A. Nagoya, K. Okamoto, I. Tajima, R. Ohta, A. Okamoto, Optically tunable amino-functionalized graphene quantum dots, Adv. Mater. 24 (2012) 5333–5338.
[47] Y. Li, Y. Zhao, H. Cheng, Y. Hu, G. Shi, L. Dai, L. Qu, Nitrogen-doped graphene quantum dots with oxygen-rich functional groups, J. Am. Chem. Soc. 134 (2012) 15–18.
[48] J. Long, X. Xie, J. Xu, Q. Gu, L. Chen, X. Wang, Nitrogen-doped graphene nanosheets as metal-free catalysts for aerobic selective oxidation of benzylic alcohols, ACS Catal. 2 (2012) 622–631.
[49] Y. Dong, J. Shao, C. Chen, H. Li, R. Wang, Y. Chi, X. Lin, G. Chen, Blue luminescent graphene quantum dots and graphene oxide prepared by tuning the carbonization degree of citric acid, Carbon 50 (2012) 4738–4743.
[50] J. Xu, G. Dong, C. Jin, M. Huang, L. Guan, Sulfur and nitrogen co-doped, few-layered graphene oxide as a highly efficient electrocatalyst for the oxygen-reduction reaction, Chem. Sus. Chem. 6 (2013) 493–499.
[51] S. Glenis, A.J. Nelson, M.M. Labes, Sulfur doped graphite prepared via arc discharge of carbon rods in the presence of thiophenes, J. Appl. Phys. 186 (1999) 4464–4466.
[52] D. Qu, M. Zheng, P. Du, Y. Zhou, L. Zhang, D. Li, H. Tan, Z. Zhao, Z. Xie, Z. Sun, Highly luminescent S, N co-doped graphene quantum dots with broad visible absorption bands for visible light photocatalysts, Nanoscale 5 (2013) 12272–12277.
[53] Y. Dong, H. Pang, H.B. Yang, C. Guo, J. Shao, Y. Chi, C.M. Li, T. Yu, Carbon-based dots co-doped with nitrogen and sulfur for high quantum yield and excitation-independent emission, Angew. Chem. In. Ed. 52 (2013) 7800–7804.
[54] A.M. Roy, G.C. De, N. Sasmal, S.S. Bhattacharyya, Determination of the flatband potential of semiconductor particles in suspension by photovoltage measurement, Int. J. Hydrogen Energy 20 (1995) 627–630.
[55] M. Long, P. Hu, H. Wu, Y. Chen, B. Tan, W. Cai, Understanding compositions and electronic structures dependent photocatalytic performance of bismuth oxyiodides, J. Mater. Chem. A 3 (2015) 5592–5598.
[56] H. Bader, V. Sturzenegger, J. Hoigné, Photometric method for the determination of low concentrations of hydrogen peroxide by the peroxidase catalyzed oxidation of N,N-diethyl-p-phenylenediamine (DPD), Water Res. 22 (1988) 1109–1115.
[57] J.K. Nørskov, J. Rossmeisl, A. Logadottir, L. Lindqvist, J.R. Kitchin, T. Bligaard, H. Jónsson, Origin of the overpotential for oxygen reduction at a fuel-cell cathode, J. Phys. Chem. B 108 (2004) 17886–17892.
[58] D. Qu, Z. Sun, M. Zheng, J. Li, Y. Zhang, G. Zhang, H. Zhao, X. Liu, Z. Xie, Three colors emission from S, N co-doped graphene quantum dots for visible light H_2 production and bioimaging, Adv. Opt. Mater. 3 (2015) 360–367.
[59] P. Hu, H. Su, Z. Chen, C. Yu, Q. Li, B. Zhou, P.J.J. Alvarez, M. Long, Selective degradation of organic pollutants using an efficient metal-free catalyst derived from carbonized polypyrrole via peroxymonosulfate activation, Environ. Sci. Technol. 51 (2017) 11288–11296.
[60] H. Fei, J. Dong, M.J. Arellano-Jime´nez, G. Ye, N.D. Kim, E.L.G. Samuel, Z. Peng, Z. Zhu, F. Qin, J. Bao, M.J. Yacaman, P.M. Ajayan, D. Chen, J.M. Tour, Atomic cobalt on nitrogen-doped graphene for hydrogen generation, Nat. Commun. 6 (2015) 8668–8675.
[61] C. Chen, Z. Zhou, Y. Wang, X. Zhang, X. Yang, X. Zhang, S. Sun, N. Fe, S-doped porous carbon as oxygen reduction reaction catalyst in acidic medium with high activity and durability synthesized using $CaCl_2$ as template, Chin. J. Catal. 38 (2017) 673–682.
[62] A. Fujishima, X. Zhang, D.A. Tryk, TiO_2 photocatalysis and related surface phenomena, Surf. Sci. Rep. 63 (2008) 515–582.
[63] A. Imanishi, T. Okamura, N. Ohashi, R. Nakamura, Y. Nakato, Mechanism of Water photooxidation reaction at atomically flat TiO_2 (rutile) (110) and (100) surfaces: dependence on solution pH, J. Am. Chem. Soc. 129 (2007) 11569–11578.
[64] M. Long, J. Brame, F. Qin, J. Bao, Q. Li, P.J.J. Alvarez, Phosphate changes effect of humic acids on TiO_2 photocatalysis: from inhibition to mitigation of electron–hole recombination, Environ. Sci. Technol. 51 (2017) 514–521.
[65] H. Sheng, Q. Li, W. Ma, H. Ji, C. Chen, J. Zhao, Photocatalytic degradation of organic pollutants on surface anionized TiO_2: common effect of anions for high hole-availability by water, Appl. Catal. B: Environ. 138–139 (2013) 212–218.
[66] M. Kotal, J. Kim, K.J. Kim, I.K. Oh, Sulfur and nitrogen co-doped graphene electrodes for high-performance ionic artificial muscles, Adv. Mater. 28 (2016) 1610–1615.
[67] Y. Tian, Y. Ma, H. Liu, X. Zhang, W. Peng, One-step and rapid synthesis of nitrogen and sulfur co-doped graphene for hydrogen peroxide and glucose sensing, J. Electro. Chem. 742 (2015) 8–14.
[68] Z. Qiang, J.H. Chang, C.P. Huang, Electrochemical generation of hydrogen peroxide from dissolved oxygen in acidic solutions, Water Res. 36 (2002) 85–94.
[69] H. Xia, J. Zhang, Z. Yang, S. Guo, S. Guo, Q. Xu, 2D MOF nanoflake-assembled spherical microstructures for enhanced supercapacitor and electrocatalysis performances, Nano-Micro Lett. 9 (2017) 43.
[70] W. Chen, J. Kim, S.H. Sun, S.W. Chen, Electrocatalytic reduction of oxygen by FePt alloy nanoparticles, J. Phys. Chem. C 112 (2008) 3891–3898.
[71] X. Duan, H. Sun, S. Wang, Metal-free carbocatalysis in advanced oxidation reactions, Acc. Chem. Res. 51 (2018) 678–687.
[72] X. Duan, K. O'Donnell, H. Sun, Y. Wang, S. Wang, Sulfur and nitrogen co-doped graphene for metal-free catalytic oxidation reactions, Small 11 (2015) 3036–3044.
[73] T.A. Tripolskaya, I.V. Pokhabova, P.V. Prikhodchenko, G.P. Pilipenko, E.A. Legurova, N.A. Chumaevskii, Identification of peroxo groups in supramolecular layered structures as probed by Raman spectroscopy, Russ. J. Inorg. Chem. 54 (2009) 464–466.